Protonation State of Glu142 Differs in the Green- and Blue-Absorbing Variants of Proteorhodopsin[†]

Joel M. Kralj,[‡] Vladislav B. Bergo,[‡,§] Jason J. Amsden,[‡] Elena N. Spudich,[§] John L. Spudich,[§] and Kenneth J. Rothschild*[,‡]

Department of Physics, Molecular Biophysics Laboratory and Photonics Center, Boston University, Boston, Massachusetts 02215, and Center for Membrane Biology, Department of Biochemistry and Molecular Biology, University of Texas Medical School, Houston, Texas 77030

Received September 17, 2007; Revised Manuscript Received December 23, 2007

ABSTRACT: Proteorhodopsins are a recently discovered class of microbial rhodopsins, ubiquitous in marine bacteria. Over 4000 variants have thus far been discovered, distributed throughout the oceans of the world. Most variants fall into one of two major groups, green- or blue-absorbing proteorhodopsin (GPR and BPR, respectively), on the basis of both the visible absorption maxima (530 versus 490 nm) and photocycle kinetics (∼20 versus ∼200 ms). For a well-studied pair, these differences appear to be largely determined by the identity of a single residue at position 105 (leucine/GPR and glutamine/BPR). We find using a combination of visible and infrared spectroscopy that a second difference is the protonation state of a glutamic acid residue located at position 142 on the extracellular side of helix D. In BPR, Glu142 (the GPR numbering system is used) is deprotonated and can act as an alternate proton acceptor, thus explaining the earlier observations that neutralization of the Schiff base counterion, Asp97, does not block the formation of the M intermediate. In contrast, Glu142 in GPR is protonated and cannot act in this state as an alternate proton acceptor for the Schiff base. On the basis of these findings, a mechanism is proposed for proton pumping in BPR. Because the pK_a of Glu142 is near the pH of its native marine environment, changes in pH may act to modulate its function in the cell.

Microbial rhodopsins are photoactive membrane proteins found in diverse organisms including the domains of archaea (*1*), eubacteria (*2*), and lower eukaryotes (*3*). Functioning as ion pumps or light sensors (*4*), these molecules can differ significantly in primary structure. However, they all share a seven transmembrane α-helix motif with a retinylidene chromophore attached to a lysine in helix G through a protonated Schiff base (SB).[1] A highly conserved carboxylate group located in helix C serves as the SB counterion and proton acceptor during the photocycle, although exceptions exist, such as halorhodopsin, which has no such counterion, and *Halobacterium salinarum* sensory rhodopsin I, which has the conserved aspartate residue but it is protonated in the dark and therefore does not function as a counterion nor accept a proton from the SB (*4*).

Proteorhodopsin is a recently discovered class of microbial rhodopsins originally found in γ-proteobacteria (*2, 5*). Since its detection, over 4000 variants have been found using a variety of genomic techniques (*6–8*). Several variants have been cloned into *Escherichia coli*, with the two most intensively studied forms being members of the dominant classes: green-absorbing proteorhodopsin (GPR) and blue-absorbing proteorhodopsin (BPR).

Previous studies have established that GPR has properties similar to bacteriorhodopsin (BR), including light-driven proton pumping, a fast photocycle (20 ms), and a red-shifted visible absorption maximum (532 nm) (*9–11*). BPR, in contrast, has a similar primary structure but a blue-shifted visible max near 490 nm and a slower photocycle (∼200 ms) (*5, 12, 13*). Although it has also been shown to pump protons at high pH, the slower photocycle leads to inefficient proton pumping, and the possibility has been raised that BPR may have a regulatory rather than energy-harvesting role in the cell (*13*). Recently, a study using homology modeling and energy minimization suggested that, at high pH, the tertiary structure of BPR is more accurately modeled by sensory rhodopsin II (SRII) rather than BR (*14*).

This study used time-resolved Fourier transform infrared (FTIR) and visible spectroscopy to examine the molecular differences between the blue- and green-absorbing forms of proteorhodopsin (see Figure 1 for sequence differences). On the basis of these measurements, we propose that Glu142 is normally deprotonated in the unphotolyzed state of BPR at a pH above 7, whereas in GPR, this residue is protonated [the numbering scheme for BPR is offset by one from GPR because of a glycine at residue 2 (Figure 1)]. This paper uses the GPR numbering throughout. During the late stage of the photocycle, a band appears at 1767 cm^{-1} in BPR unlike other rhodopsin-like proton pumps, which may correspond to protonation of Glu142. Because the pK_a of

[†] This work was supported by National Institutes of Health Grants R01GM069969 (to K.J.R.) and R37GM27750 (to J.L.S.), Department of Energy Grant DE-FG02-07ER15867, and the Robert A. Welch foundation (to J.L.S.).

* To whom correspondence should be addressed: Department of Physics, 590 Commonwealth Avenue, Boston, MA 02215. Fax: 617-353-9393. E-mail: kjr@bu.edu.

[‡] Boston University.

[§] University of Texas Medical School.

10.1021/bi7018964 CCC: $40.75
Published on Web 02/20/2008

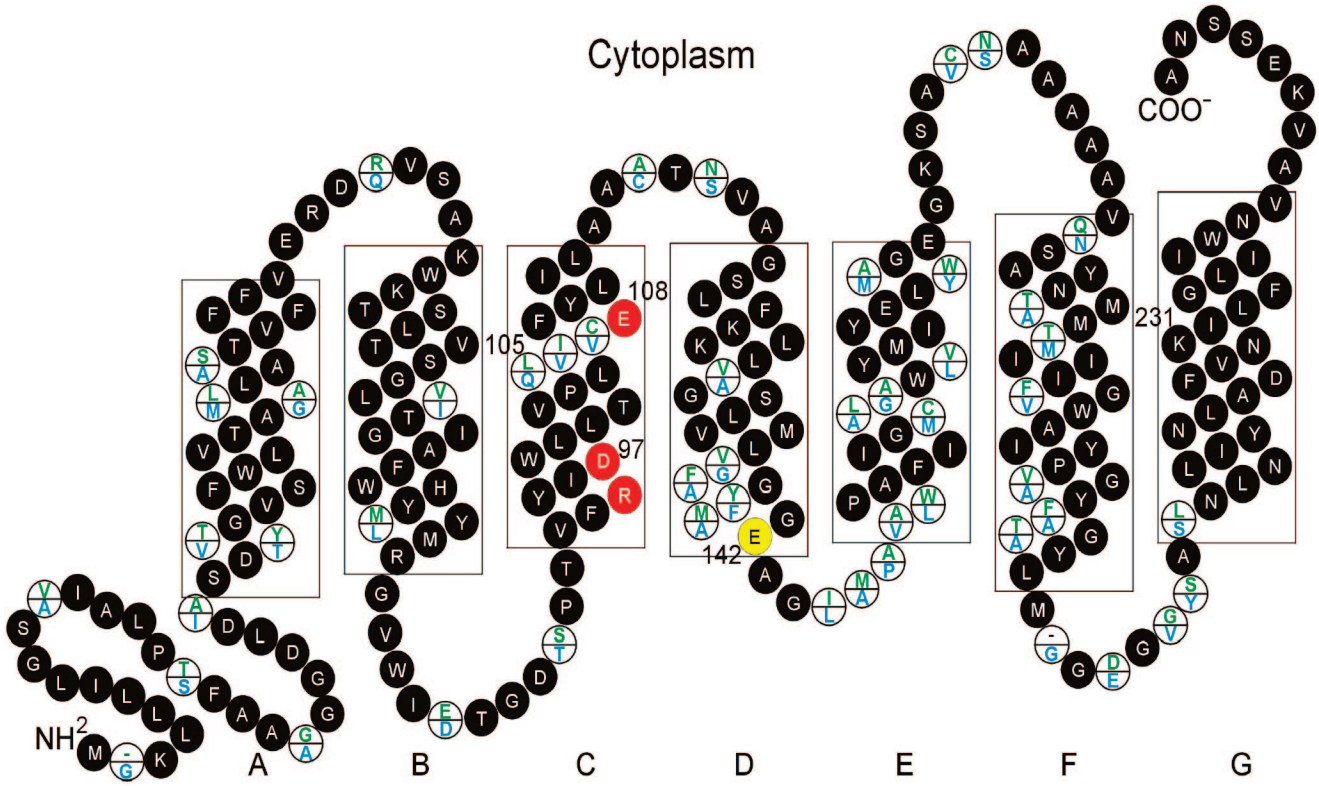

FIGURE 1: Snake diagram comparing the secondary structures of GPR and BPR taken from ref *5*. All numbering is based on the GPR sequence. Solid circles indicate residues identical in both species. White circles indicate positions where amino acid identity differs with the GPR amino acid on top (green) and BPR amino acid on bottom (blue). A−G indicate helix designations. Red circles indicate important residues implicated in the proteorhodopsin proton pump. Glu142 is shown in yellow.

Glu142 in BPR (but not GPR) is near the pH expected for typical marine environments, its protonation state may play a role in cellular regulation, which might be different from GPR as previously suggested (*13, 14*).

EXPERIMENTAL PROCEDURES

Protein Expression and Purification. All procedures for the site-directed mutagenesis, plasmid construction, and expression in the *E. coli* UT5600 strain were similar to those described previously (*15*). After the induction period, the cells expressing His-tagged wild-type (WT) or mutant GPR (BAC31A08) and BPR (HOT75M4) were centrifuged at 1000*g*, resuspended in 5 mM $MgCl_2$ and 150 mM Tris-HCl at pH 7.0, and disrupted by sonication. Unbroken cells were removed by low-speed centrifugation. The membranes containing pigment were collected by centrifugation (39000*g* for 30 min) and solubilized in a wash buffer [50 mM KP_i, 300 mM NaCl, 5 mM imidazole, and 1.5% octylglucoside (OG) at pH 7.0] for at least 1 h at 4 °C. Unsolubilized membranes were removed by centrifugation at 28000*g* for 30 min. The supernatant was incubated with a His-binding resin on a shaker at 4 °C for at least 1 h. The bound resin was applied to a 10 cm chromatography column and washed with 3× volume of wash buffer followed by elution buffer (50 mM KP_i, 300 mM NaCl, 250 mM imidazole, and 1.0% OG at pH 7.0). The sample purity was assessed by UV–vis spectroscopy (*2*).

Proteoliposome Reconstitution. Purified His-tagged PR was reconstituted in *E. coli* polar lipids (Avanti, Alabaster, AL) at a 1:10 protein/lipid (w/w) ratio. Lipids initially dissolved in chloroform were dried under argon and resuspended in dialysis buffer (50 mM K phosphate and 300 mM NaCl at pH 7.0), to which OG was added to a final concentration of 1%. The lipid solution was incubated with OG-solubilized protein for 1 h on ice and dialyzed against dialysis buffer with three buffer changes every 24 h. The reconstituted protein was centrifuged for 15 min and resuspended in sample buffer at least 2 times [50 mM 2-(cyclohexylamino)ethylsulfonic acid (CHES) and 150 mM NaCl at pH 9.5].

FTIR Measurements. Protein films for rapid-scan FTIR measurements were prepared by depositing 15–20 μL of the proteoliposome suspension onto a polished 2 mm thick, 25 mm diameter CaF_2 window (Wilmad, Buena, NJ) and drying the sample under a gentle stream of argon. Films were rehydrated via the vapor phase and then sealed in a temperature-controlled IR cell (Model TFC, Harrick Scientific Corp., Ossining, NY) using a second CaF_2 window. Spectra were recorded with a Bruker IFS 66 v/s FTIR spectrometer (Bruker Optics, Germany) as described previously (*16*) at 4 cm^{-1} spectral resolution and 240 kHz scanner velocity, corresponding to the data acquisition window of 18 ms. Four single-beam spectra were recorded before the laser flash and were used as the "dark" background. A Nd/YAG laser pulse initiated the photocycle, and 80 "light" spectra were recorded with each acquisition, taking 18 ms. Spectra taken in this sequence were co-added 20 000 times to achieve a high signal-to-noise ratio. The first four "light" spectra collected within 60 ms after initiation of the photocycle were averaged, from which the dark spectrum was subtracted to yield a light minus dark IR spectrum. All spectra were recorded at 5 °C unless otherwise specified.

Low-temperature measurements were the same as reported before (*17*). Approximately 200 μg of the protein was deposited on CaF_2 windows and dried under a slow stream of argon. Samples were hydrated via the vapor phase and sealed in a sample cell with another CaF_2 window. Difference spectra were recorded at 2 cm^{-1} resolution using a Bio-Rad FTS-60A FTIR spectrometer (Bio-Rad, Digilab Division, Cambridge, MA) equipped with a liquid-nitrogen-cooled MCT detector. A Dolan-Jenner (Woburn, MA) model 180 illuminator (150 W, tungsten−halogen) and a fiber-optic light guide were used for sample illumination in combination with 500 nm low-pass and 570 nm long-pass optical filters (Corion Corp., Holliston, MA). Difference spectra were obtained at 80 K as previously described for BR (*18*). All measurements were performed on at least two independently prepared samples to ensure that the observed spectra were reproducible.

Visible Spectra Measurements. Visible spectra data were taken on a HP 8453 visible spectrometer. Protein samples were solubilized in 20% OG and then diluted 10:1 with the specified pH buffer for a final concentration of 2% OG. The baseline was corrected by fitting a quartic function to account for Rayleigh scattering. Titration data was taken with 2 mL of protein in a cuvette with a stir bar. Acid or base was added in 2 μL steps to avoid dilution of the sample. The resulting spectra were decomposed using the single-value decomposition (SVD) function in MATLab (Mathworks, Natick, MA). The resulting spectra were fit to the function. $y = 1 - A/(1 + 10^{(pH-pK_a)})$ In the case of BPR, two separate pK_a values were fit using the function $y = 1 - A/(1 + 10^{(pH-pK_{a1})}) - B/(10^{(pH-pK_{a2})})$, where y represents the percent of the protonated form and A and B are fitting parameters.

Homology Modeling. The secondary-structure model presented in Figure 1 was taken from Beja et al. (*5*) using the numbering from GPR to maintain clarity. Both the alignment of the helices as well as the residues are presented in the reference. The 3D model in Figure 8 uses SRII as the basis (Protein Data Bank ID number 1JGJ) from ref *19*. The BPR residues were imported to minimize steric interactions with the surrounding residues only. This model is only presented to provide a possible pathway and does not represent the free-energy minima of the protein.

RESULTS

Neutralizing Asp97 Does Not Block the Late Photocycle in BPR. Previously, it has been shown in BR and GPR that the replacement of the proton acceptor group (Asp85 and Asp97, respectively) with a neutral Asn residue almost completely blocks the formation of the M intermediate (*15, 20*). Instead, a much faster photocycle is observed where a red-shifted K-like intermediate is formed and rapidly decays to the original state (*15*). In contrast, the homologous substitution in BPR does not eliminate M formation, implying that an alternate proton acceptor exists in this proteorhodopsin variant (*13*). This is supported by visible absorption pH titration experiments, which reveal that in GPR there exists a single group, Asp97, with a pK_a near 7.6 (*13, 15*) whose protonation causes the acid-induced red shift in visible absorption, whereas in BPR, there are two groups with pK_a values at 6.5 and 7.7, which cause the red shift of the visible absorption (*13, 14*).

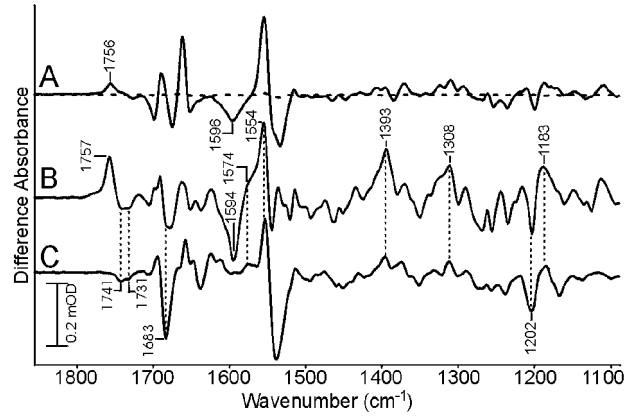

FIGURE 2: FTIR difference spectrum of (A) GPR WT (—) and D97N mutant (- - -) averaged from 5 to 50 ms, (B) BPR WT averaged from 5 to 50 ms, and (C) BPR D97N mutant averaged from 5 to 50 ms. No evidence is seen for a GPR D97N photocycle within our time resolution (18 ms) at 5 °C. Note that the scale marker applies to all spectra.

In agreement with previous results, our FTIR difference spectrum of the GPR D97N mutant shows no detectable difference bands within our time-resolution window (18 ms), indicating that the photocycle is already completed in contrast to the WT pigment (Figure 2A), in which a slower photocycle is detected. The observed WT FTIR difference spectrum is very similar to that previously published (*20*). Unlike GPR, the spectra of BPR WT and the BPR D97N mutant (parts B and C of Figure 2) both exhibit bands indicative of the formation of late photointermediates. For example, bands in the wild-type spectrum characteristic of the M intermediate including bands at 1574(+) are still present in D97N, demonstrating that this mutant forms M. In addition, positive bands attributed to the N intermediate are present at 1554, 1393, 1308, and 1183 cm^{-1}. However, in contrast to the WT, D97N spectra do not exhibit peaks characteristic of the O intermediates (1535/1167 cm^{-1}) (Kralj and Rothschild, to be published), even as late as 1.5 s.

The most noticeable change in the BPR D97N mutant compared to the WT is the disappearance of the bands at 1757(+) and 1594(−) cm^{-1}. On the basis of this mutant and the similarity of the band to GPR at 1755 cm^{-1} (*15*) and BR at 1761 cm^{-1} (*20, 21*), these bands are assigned to the protonated [1757(+) cm^{-1}] and unprotonated [1594(−) cm^{-1}] forms of the Asp97 counterion carboxylic acid group. Note that similar bands appear in the GPR difference spectra at 1756(+) and 1596(−) cm^{-1} but cannot be assigned on the basis of the D97N mutation because it does not form M. However, the 1756 cm^{-1} band was assigned previously on the basis of the D97E mutant, which downshifts its frequency (*15*). The other bands in the COOH region of BPR are still present in the D97N mutant, except for the high-frequency 1768 cm^{-1} band (see below). Hence, unlike GPR, neutralization of Asp97 does not prevent deprotonation of the SB, although the late photocycle is altered. This observation supports the proposal based on absorption spectral titrations and flash photolysis that there exists an alternate proton acceptor (*13*).

Neutralizing Glu142 in BPR Abolishes the Anomalous pH-Induced Red Shift. A recent study suggested that residue 142 in BPR plays a key role in the color-tuning mechanism (*14*). BPR exhibits one of the largest acid-induced red shifts of

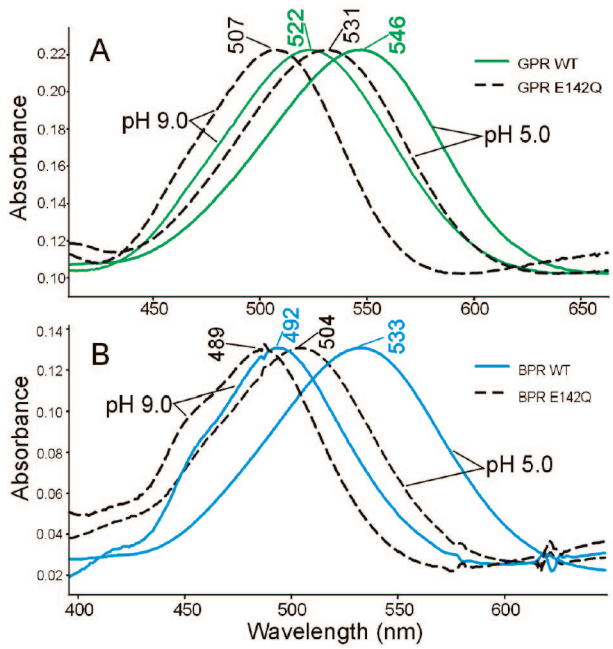

FIGURE 3: Visible absorption of (A) GPR WT and GPR E142Q and (B) BPR WT and BPR E142Q at pH 9 and 5. In GPR E142Q, it is blue-shifted by the same amount at both high and low pH (15 nm). However, in BPR, the mutant and WT have nearly identical absorption at pH 9 but differ considerably at pH 5, suggesting a difference between high and low pH forms at residue Glu142.

all microbial rhodopsins (~41 nm, see Figure 3A). This red shift is generally attributed to the neutralization of the SB counterion, which on the basis of a simple point-charged model is expected to result in a red shift of the visible absorption (*22*). To explain the much larger red shift in BPR compared to other microbial rhodopsins including GPR, it was predicted on the basis of model calculations (*14*) that Glu142 is deprotonated in BPR and forms a salt bridge with Arg94 at high pH but becomes neutralized at lower pH, resulting in the movement of Arg94 toward the Asp97 counterion to form a complex counterion structure similar to that of BR (*23*).

To test this model, mutants were made replacing Glu142 with a neutral glutamine in both GPR and BPR (E142Q). Parts A and B of Figure 3 show the visible absorption spectra of the WT and mutants of GPR and BPR at both high and low pH in 2% OG. In the case of GPR (Figure 3A), a similar acid-induced red shift of 24 nm occurs in both the WT and mutant E142Q, although the overall absorption maxima of the low and high pH forms of the mutant are lowered by 15 nm relative to the WT. This result indicates that the charge of Glu142 has little effect on the previously characterized GPR acid-induced red shift attributed to protonation of Asp97 (*5, 11, 12, 15*). In contrast, in the case of BPR (Figure 3B), the much larger acid-induced red shift of 41 nm in the WT is reduced to only 15 nm in the case of the E142Q mutant. This result indicates that the anomalously large acid-induced red shift in BPR involves the neutralization of Glu142 as previously predicted (*14*).

Identification of Glu142 as the Second Residue Involved in the Acid-Induced Red Shift of BPR. Unlike most microbial rhodopsins, such as BR and GPR, which exhibit a single pK_a for the absorption spectrum shift because of the protonation of the SB counterion, BPR exhibits two inflection points in the pH titration curve (*13, 24*). In addition,

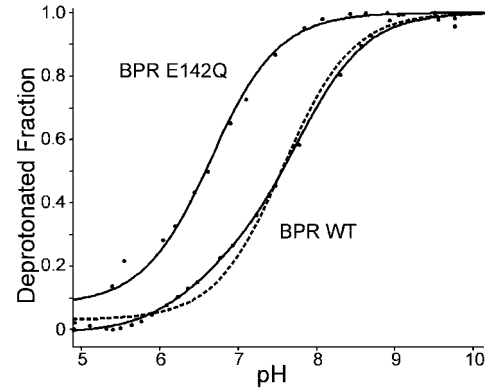

FIGURE 4: Visible absorption maximum versus pH (pH titration curve) of BPR WT and BPR E142Q. The fit for a single pK_a value of the BPR WT is the dashed line, and for two pK_a values, the fit is solid. Similar to previous results, the BPR WT was not well-fit by a single pK_a but was for two values of pK_a at 6.5 and 7.7. In contrast, the E142Q mutant fit to a single pK_a at 6.7.

neutralization of the Asp97 counterion in BPR does not completely eliminate the color shift between high and low pH as it does in GPR (*13, 15*). This evidence suggests that a second protonatable residue is involved in the acid-induced red shift.

A visible titration experiment was performed on the GPR WT, BPR WT, and BPR E142Q mutant to determine if Glu142 is responsible for the second pK_a observed. Data were analyzed using SVD, and the resulting decay traces fit to either one or two pK_a values. As expected, the GPR WT fit to a single pK_a at 7.5, similar to earlier studies (data not shown) (*11, 15*). However, BPR WT does not fit well to a single pK_a value, resulting in a root-mean-square (rms) error of 3.4% (Figure 4). Using two pK_a values, the fitting produced values at 6.5 and 7.7 with a significantly improved fit (rms error of 0.9%) similar to an earlier study, which predicted pK_a values at 6.2 and 7.8 (*13*). In contrast, the mutant E142Q data can be fit with only a single pK_a at 6.6 (rms error of 1.0%). These results strongly indicate that Glu142 is the likely cause of the second inflection point in the titration curve and that it undergoes protonation in the same range as Asp97. Because the E142Q mutant exhibits a single pK_a at 6.6, it appears that the second, higher pK_a measured for WT at 7.7 is due to Glu142. This result is consistent with the titration data on the D97N mutant, which reveals that this mutant has a single pK_a near 7.1 (*13*).

Neutralization of Glu142 Results in a Slowly Decaying K-like Intermediate. To further investigate the role of Glu142 during the BPR photocycle, we used FTIR difference spectroscopy, which is sensitive to both retinal and protein changes. Parts A and B of Figure 5 show the FTIR difference spectra of GPR and BPR E142Q mutants measured at pH 9.5 (—) as compared to the corresponding WT spectra (•••) measured under similar conditions. In the case of GPR E142Q (Figure 5A), the mutation produces only limited changes relative to the WT. In particular, peaks in the COOH region [1756(+), 1742(+), and 1728(−) cm^{-1}], reflecting protonation changes, and the retinal fingerprint region (1253(−), 1234(−), and 1198(−) cm^{-1}], reflecting the retinal C−C stretching modes, are nearly identical. The largest changes are a reduction in the intensity of bands in the amide I region at 1674, 1661, and 1650 cm^{-1}, which most likely

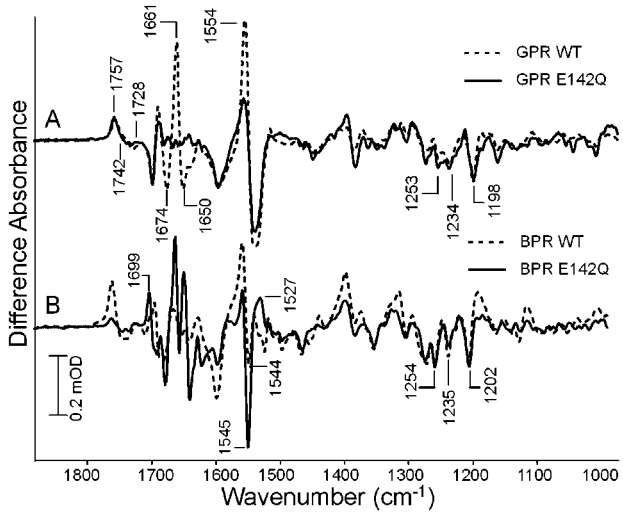

FIGURE 5: Difference spectra of (A) GPR WT (- - -) and E142Q mutant (—) and (B) BPR WT (- - -) and E142Q mutant (—), all averaged from 5 to 50 ms. The GPR mutant has little effect, while the BPR mutant drastically alters the photocycle, especially at 1699 and 1527 cm^{-1}. Note that the scale marker applies to all spectra.

reflect an inhibition of structural changes in the GPR backbone in the late photocycle for E142Q.

In contrast, the corresponding BPR E142Q mutant (Figure 5B) exhibits a highly perturbed difference spectrum, indicating an altered photocycle from the WT. Bands reflecting the protein backbone, carboxylic acids, and retinal chromophore are all affected upon neutralization of this residue. Most notable are positive bands appearing in BPR E142Q at 1699, 1527, and 1189 cm^{-1}, characteristic of the red-shifted K intermediate of BPR (Amsden and Rothschild, to be published). Especially notable is the positive band at 1699 cm^{-1}, which in the case of the GPR K intermediate has been assigned to perturbation of Asn230 located next to Lys231, whose side-chain nitrogen is a component of the retinal SB (*17*). The fact that these bands are visible after 50 ms indicates that the K-like intermediate decay is drastically slowed in this mutant. The reduced intensity of the 1757 cm^{-1} band (Figure 5B) assigned to the protonation of the primary counterion, Asp97 (see above), also indicates that at this stage of the photocycle there is a significantly less concentration of the late photocycle intermediates (M, N, and O) formed in BPR E142Q compared to BPR WT.

Figure 6A shows the averaged early (5–50 ms) and late (200–500 ms) difference spectra for the BPR E142Q mutant. The positive bands indicative of K at 1699, 1527, and 1189 cm^{-1} have all been reduced at later times. The slow decay of a K-like intermediate can be clearly seen by comparing the double difference spectrum between the early and late times for BPR E142Q to the BPR WT K spectrum recorded at 80 K (Figure 6B). The similarity between these two confirms that the E142Q mutation dramatically slows the decay of the K-like intermediate in BPR.

Possible Protonation of Glu142 during the BPR Photocycle. Of particular interest is the COOH region from 1700 to 1800 cm^{-1}, which reflects the protonation of carboxylic acid residues. In BPR WT, at high pH, bands are seen at 1768(+), 1757(+), 1741(−), 1731(−), 1719(+), and 1704(−) cm^{-1} (Figure 7). The 1757(+) cm^{-1} band is assigned to protonation of the Asp97 proton-donor group during M formation, as discussed above. As shown elsewhere, the

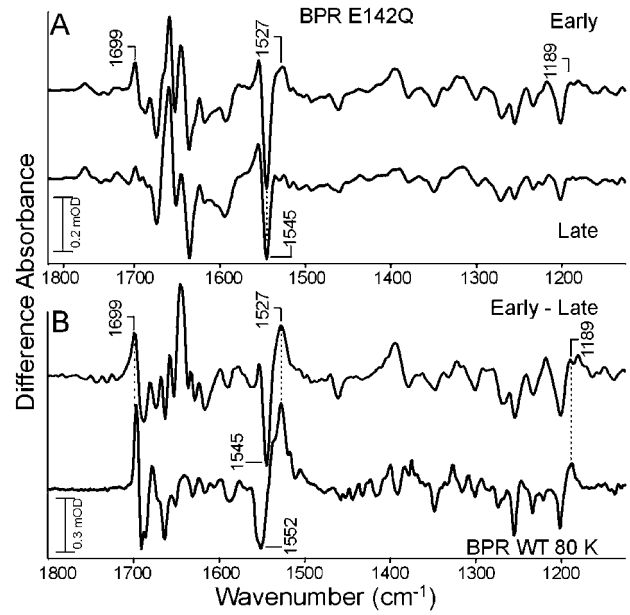

FIGURE 6: (A) Early (5–50 ms) and late (200–500 ms) time averages of the BPR E142Q mutant. (B) Double difference spectrum of the E142Q mutant compared to the WT K spectrum acquired at 80 K. The early−late spectrum closely resembles the LT K spectrum, showing that a K-like spectrum is observed even at times as late as 50 ms.

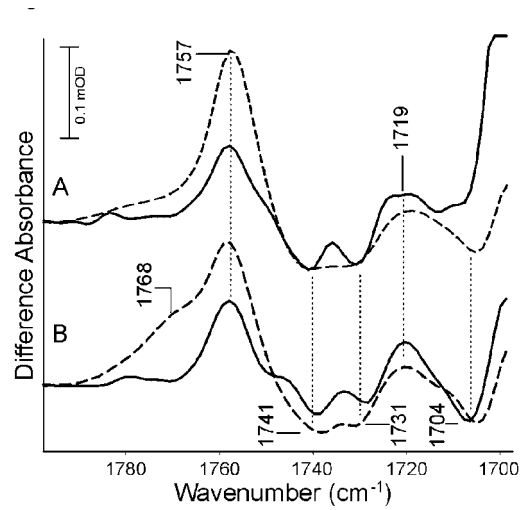

FIGURE 7: Carboxylic acid region of BPR WT (- - -) and BPR E142Q (—) averaged over the time interval (A) 5–50 and (B) 200–500 ms. There is no evidence of the late 1768 cm^{-1} band in the E142Q mutant. All other bands found in the WT spectrum also appear in the mutant in this region of the spectrum. Note that the scale marker applies to all spectra.

1731(−) cm^{-1} band is assigned to deprotonation of the SB-donor group Glu108 and the 1741(−) cm^{-1} band is assigned to deprotonation of Glu214, which may function as the proton-ejection group to the extracellular medium (*25*).

The 1768(+) cm^{-1} band seen as a shoulder (Figure 7B) grows in during the late photocycle after the decay of M as indicated by the reduction in intensity of the 1757(+) cm^{-1} band. In contrast, this change is absent in the mutant E142Q.

One possible interpretation is that the 1768(+) cm^{-1} band arises from the protonation of Glu142 during the late photocycle, coincident with the formation of the O intermediate. This would explain the appearance of this high-frequency carboxylic band, which is not seen in GPR or other

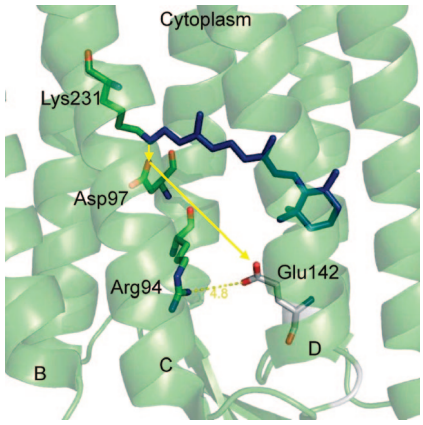

FIGURE 8: Structure of BPR modeled on the 3D crystal structure of SRII (1JGJ) from ref *19*. BPR residues were imported by minimizing steric interactions. A negatively charged Glu142 is in a position to interact with the positive charge of Arg94, located 4.8 Å away. The yellow arrows indicate the proposed proton pathway during the photocycle. B−D represent designated helices.

microbial rhodopsins. On the other hand, an alternative explanation is that the environment of Asp97 changes in the late photocycle, causing the upshift in frequency of the carboxylic acid stretch mode. Although a frequency shift of the band assigned to the counterion has been observed during M to N decay in other microbial rhodopsins, such as BR and GPR, it has always been a downshift (e.g., in BR, it is 1760−1755 cm^{-1}) (*15, 26*). To test the assignment of the 1768 cm^{-1} band, additional experiments will be necessary, including the use of less perturbing substitutions, such as E142D.

DISCUSSION

Several studies show that major differences in the properties of GPR and BPR can be attributed to the identity of a single residue at position 105, which is Leu105 in GPRs and Gln105 in BPRs (*12, 13, 27*). For example, substituting Gln105 for Leu105 in GPR causes a blue shift of the visible absorption from 530 to 497 nm and a much slower photocycle, whereas substituting Leu105 for Gln105 in BPR red shifts the absorption to 512 nm, although this single substitution is not sufficient to speed up the photocycle (*12, 13*). Recent Raman and low-temperature spectral studies by us (Kralj, Amsden, Spudich, Spudich, and Rothschild, to be published) reveal that these changes involve the interaction of residue 105 with the retinal SB and nearby C13 methyl group. In particular, in the case of BPR, Gln105 is directly hydrogen-bonded to the SB, whereas in GPR, this interaction is replaced by a water molecule. It is known that water molecules play an important role in the BR proton release (*28*), and a more thorough examination of the water molecules in BPR will be presented in a separate paper (Amsden, Kralj, Bergo, Spudich, Spudich, and Rothschild, to be published).

In this study, we find that a second major factor, which influences the properties of GPR and BPR, is the protonation state of residue Glu142. Evidence indicates that this residue is neutral (protonated) in GPR even at pH 9, well above the normal pK_a of the Glu carboxylic acid group. In contrast, Glu142 in BPR is normally deprotonated above pH ~7.5. This difference in the protonation state of Glu142 can explain the previously observed differences between BPR and GPR, including the existence of a second SB proton acceptor and two pK_a values for the acid-induced red shift only in BPR (*13*).

On the basis of sequence alignment with the microbial rhodopsin SRII (*19*), residue 142 is located on helix D near the extracellular side of the membrane over 13 Å from the SB but close enough to interact with the positively charged Arg94 (Figure 8), as previously hypothesized (*14*). An important question is whether protonation of Glu142 occurs during the BPR photocycle. For example, as shown in Figure 8, protonation of the Schiff base counterion Asp97 upon M formation could be followed by movement of this proton to Glu142, thereby triggering a disruption of the Arg94 salt bridge and subsequent proton ejection to the extracellular medium. The disruption of an Arg−carboxylate salt bridge is analogous to the role originally proposed for the homologous residue, Arg82, located in the BR helix C on the basis of spectroscopic measurements (*29*) and more recently confirmed by X-ray crystallographic studies (*30*). In this model, protonation of the SB counterion, Asp85, causes a movement of Arg82 away from the counterion and toward the cytoplasmic medium, thereby triggering proton ejection. However, in the case of BPR, this movement of Arg94 is caused by the disruption of its salt bridge with the secondary counterion Glu142 after a proton is transferred from the primary counterion Asp97. A similar conclusion of two separate counterions has been observed in bovine rhodopsin. There, Glu181 becomes the SB counterion only in the light activated meta-I state, implying a counterion switch (*31*).

Consistent with this model, we find evidence for the near simultaneous deprotonation of Asp97 and protonation of Glu142 during the BPR photocycle. In particular, an unusually high-frequency band at 1768 cm^{-1} appears in the late photocycle of BPR, which can be assigned to protonation of a carboxylate group. A simultaneous decrease in intensity of a band at 1757 cm^{-1} assigned to the protonated state of Asp97 is observed, consistent with its deprotonation. However, the definitive assignment of the high-frequency 1768 cm^{-1} band to Glu142 requires additional studies combining FTIR and site-directed mutagenesis.

Our results also show that BPR exhibits three distinctive photocycles depending upon the pH. At high pH, the late intermediates look similar to those of BR, with a distinct N to O photocycle transition. It therefore is likely that, at a pH above the pK_a values of both Asp97 and Glu142, BPR acts as an ion pump, ejecting a proton to the extracellular medium. However, at an intermediate pH, between 7.5 and 6.5, when some fraction of Glu142 is protonated but Asp97 is not, a completely different photocycle is observed, characterized by a slowed K-like intermediate decay and the formation of late photocycle intermediates. Finally, at an even lower pH, BPR has a very fast photocycle, characteristic of the acid-induced red form of most microbial rhodopsins.

It is possible that under the intermediate pH conditions between 6.5 and 7.5, where Glu142 is protonated but Asp97 is not, the function of BPR changes. For example, it has previously been suggested that BPR may serve a regulatory rather than energy-harvesting function (*13, 14*). Possibly, it serves both, with a sensory function occurring only if the pH is sufficiently low in the marine environment. Because species of proteobacteria containing BPR tend to be found significantly offshore, away from high-nutrient areas (*8*),

BPR may have evolved an ability to switch to a sensory function in response to its low-nutrient environment.

REFERENCES

1. Oesterhelt, D., and Stoeckenius, W. (1973) Functions of a new photoreceptor membrane. *Proc. Natl. Acad. Sci. U.S.A. 70* (10), 2853–2857.
2. Beja, O., Aravind, L., Koonin, E. V., Suzuki, M. T., Hadd, A., Nguyen, L. P., Jovanovich, S. B., Gates, C. M., Feldman, R. A., Spudich, J. L., Spudich, E. N., and DeLong, E. F. (2000) Bacterial rhodopsin: Evidence for a new type of phototrophy in the sea. *Science 289*, 1902–1906.
3. Bieszke, J. A., Spudich, E. N., Scott, K. L., Borkovich, K. A., and Spudich, J. L. (1999) A eukaryotic protein, NOP-1, binds retinal to form an archaeal rhodopsin-like photochemically reactive pigment. *Biochemistry 38*, 14138–14145.
4. Spudich, J. L. (1998) Variations on a molecular switch: Transport and sensory signalling by archaeal rhodopsins. *Mol. Microbiol. 28*, 1051–1058.
5. Beja, O., Spudich, E. N., Spudich, J. L., Leclerc, M., and DeLong, E. F. (2001) Proteorhodopsin phototrophy in the ocean. *Nature 411*, 786–789.
6. Venter, J. C., Remington, K., Heidelberg, J. F., Halpern, A. L., Rusch, D., Eisen, J. A., Wu, D., Paulsen, I., Nelson, K. E., Nelson, W., Fouts, D. E., Levy, S., Knap, A. H., Lomas, M. W., Nealson, K., White, O., Peterson, J., Hoffman, J., Parsons, R., Baden-Tillson, H., Pfannkoch, C., Rogers, Y. H., and Smith, H. O. (2004) Environmental genome shotgun sequencing of the Sargasso Sea. *Science 304*, 66–74.
7. Sabehi, G., Massana, R., Bielawski, J. P., Rosenberg, M., Delong, E. F., and Beja, O. (2003) Novel proteorhodopsin variants from the Mediterranean and Red Seas. *Environ. Microbiol. 5*, 842–849.
8. Rusch, D. B., Halpern, A. L., Sutton, G., Heidelberg, K. B., Williamson, S., Yooseph, S., Wu, D., Eisen, J. A., Hoffman, J. M., Remington, K., Beeson, K., Tran, B., Smith, H., Baden-Tillson, H., Stewart, C., Thorpe, J., Freeman, J., Andrews-Pfannkoch, C., Venter, J. E., Li, K., Kravitz, S., Heidelberg, J. F., Utterback, T., Rogers, Y. H., Falcon, L. I., Souza, V., Bonilla-Rosso, G., Eguiarte, L. E., Karl, D. M., Sathyendranath, S., Platt, T., Bermingham, E., Gallardo, V., Tamayo-Castillo, G., Ferrari, M. R., Strausberg, R. L., Nealson, K., Friedman, R., Frazier, M., and Venter, J. C. (2007) The Sorcerer II Global Ocean Sampling Expedition: Northwest Atlantic through Eastern Tropical Pacific. *PLoS Biol. 5*, e77.
9. Dioumaev, A. K., Wang, J. M., Balint, Z., Varo, G., and Lanyi, J. K. (2003) Proton transport by proteorhodopsin requires that the retinal Schiff base counterion Asp-97 be anionic. *Biochemistry 42*, 6582–6587.
10. Krebs, R. A., Alexiev, U., Partha, R., DeVita, A. M., and Braiman, M. S. (2002) Detection of fast light-activated H^+ release and M intermediate formation from proteorhodopsin. *BMC Physiol. 2*, 5.
11. Friedrich, T., Geibel, S., Kalmbach, R., Chizhov, I., Ataka, K., Heberle, J., Engelhard, M., and Bamberg, E. (2002) Proteorhodopsin is a light-driven proton pump with variable vectoriality. *J. Mol. Biol. 321*, 821–838.
12. Man, D., Wang, W., Sabehi, G., Aravind, L., Post, A. F., Massana, R., Spudich, E. N., Spudich, J. L., and Beja, O. (2003) Diversification and spectral tuning in marine proteorhodopsins. *EMBO J. 22*, 1725–1731.
13. Wang, W. W., Sineshchekov, O. A., Spudich, E. N., and Spudich, J. L. (2003) Spectroscopic and photochemical characterization of a deep ocean proteorhodopsin. *J. Biol. Chem. 278*, 33985–33991.
14. Hillebrecht, J. R., Galan, J., Rangarajan, R., Ramos, L., McCleary, K., Ward, D. E., Stuart, J. A., and Birge, R. R. (2006) Structure, function, and wavelength selection in blue-absorbing proteorhodopsin. *Biochemistry 45*, 1579–1590.
15. Dioumaev, A. K., Brown, L. S., Shih, J., Spudich, E. N., Spudich, J. L., and Lanyi, J. K. (2002) Proton transfers in the photochemical reaction cycle of proteorhodopsin. *Biochemistry 41*, 5348–5358.
16. Bergo, V. B., Spudich, E. N., Rothschild, K. J., and Spudich, J. L. (2005) Photoactivation perturbs the membrane-embedded contacts between sensory rhodopsin II and its transducer. *J. Biol. Chem. 280*, 28365–28369.
17. Bergo, V., Amsden, J. J., Spudich, E. N., Spudich, J. L., and Rothschild, K. J. (2004) Structural changes in the photoactive site of proteorhodopsin during the primary photoreaction. *Biochemistry 43*, 9075–9083.
18. Rothschild, K. J., and Marrero, H. (1982) Infrared evidence that the Schiff base of bacteriorhodopsin is protonated: bR570 and K intermediates. *Proc. Natl. Acad. Sci. U.S.A. 79*, 4045–4049.
19. Luecke, H., Schobert, B., Lanyi, J. K., Spudich, E. N., and Spudich, J. L. (2001) Crystal structure of sensory rhodopsin II at 2.4 Å: Insights into color tuning and transducer interaction. *Science 293*, 1499–1503.
20. Braiman, M. S., Mogi, T., Marti, T., Stern, L. J., Khorana, H. G., and Rothschild, K. J. (1988) Vibrational spectroscopy of bacteriorhodopsin mutants: Light-driven proton transport involves protonation changes of aspartic acid residues 85, 96, and 212. *Biochemistry 27*, 8516–8520.
21. Gerwert, K., Hess, B., Soppa, J., and Oesterhelt, D. (1989) Role of aspartate-96 in proton translocation by bacteriorhodopsin. *Proc. Natl. Acad. Sci. U.S.A. 86*, 4943–4947.
22. Honig, B., Dinur, U., Nakanishi, K., Balogh-Nair, V., Gawinowicz, M. A., Arnaboldi, M., and Motto, M. G. (1979) An external point-charge model for wavelength regulation in visual pigments. *J. Am. Chem. Soc. 101*, 7084–7086.
23. Luecke, H., Richter, H. T., and Lanyi, J. K. (1998) Proton transfer pathways in bacteriorhodopsin at 2.3 Å resolution. *Science 280*, 1934–1937.
24. Sineshchekov, O. A., and Spudich, J. L. (2004) Light-induced intramolecular charge movements in microbial rhodopsins in intact *E. coli* cells. *Photochem. Photobiol. Sci. 3*, 548–554.
25. Kralj, J. M., Amsden, J. J., Spudich, E. N., Spudich, J. L., and Rothschild, K. J. (2007) Resonance Raman spectra of blue- and green-absorbing proteorhodopsins: Evidence for different interactions of Gin/Leu 105 with the retinal c13 methyl group. *Biophys. J.* 148a–148a.
26. Braiman, M. S., Ahl, P. L., and Rothschild, K. J. (1987) Millisecond Fourier transform infrared difference spectra of bacteriorhodopsin's M412 photoproduct. *Proc. Natl. Acad. Sci. U.S.A. 84*, 5221–5225.
27. Man-Aharonovich, D., Sabehi, G., Sineshchekov, O. A., Spudich, E. N., Spudich, J. L., and Beja, O. (2004) Characterization of RS29, a blue-green proteorhodopsin variant from the Red Sea. *Photochem. Photobiol. Sci. 3*, 459–462.
28. Garczarek, F., and Gerwert, K. (2006) Functional waters in intraprotein proton transfer monitored by FTIR difference spectroscopy. *Nature 439*, 109–112.
29. Braiman, M. S., Mogi, T., Stern, L. J., Hackett, N. R., Chao, B. H., Khorana, H. G., and Rothschild, K. J. (1988) Vibrational spectroscopy of bacteriorhodopsin mutants I. Tyrosine-185 protonates and deprotonates during the photocycle. *Proteins: Struct., Funct., Genet. 3*, 219–229.
30. Lanyi, J. K. (2004) X-ray diffraction of bacteriorhodopsin photocycle intermediates. *Mol. Membr. Biol. 21*, 143–150.
31. Yan, E. C., Kazmi, M. A., De, S., Chang, B. S., Seibert, C., Marin, E. P., Mathies, R. A., and Sakmar, T. P. (2002) Function of extracellular loop 2 in rhodopsin: glutamic acid 181 modulates stability and absorption wavelength of metarhodopsin II. *Biochemistry 41*, 3620–3627.

BI7018964